Journal of Marine Science and Technology

Volume 22 | Issue 4 Article 1

ADDED MASS COMPUTATION FOR CONTROL OF AN OPEN-FRAME REMOTELY-OPERATED VEHICLE: APPLICATION USING WAMIT AND MATLAB

You-Hong Eng
Acoustic Research Laboratory, Tropical Marine Science Institute, National University of Singapore, Singapore.

Cheng-Siong Chin
School of Marine Science and Technology, Newcastle University, Newcastle upon Tyne, United Kingdom.,
cheng.chin@ncl.ac.uk

Michael Wai-Shing Lau
School of Mechanical and Systems Engineering, Newcastle University, Newcastle upon Tyne, United Kingdom.

Follow this and additional works at: https://jmstt.ntou.edu.tw/journal

 Part of the Controls and Control Theory Commons

Recommended Citation

Eng, You-Hong; Chin, Cheng-Siong; and Lau, Michael Wai-Shing (2014) "ADDED MASS COMPUTATION FOR CONTROL OF AN OPEN-FRAME REMOTELY-OPERATED VEHICLE: APPLICATION USING WAMIT AND MATLAB," *Journal of Marine Science and Technology*: Vol. 22 : Iss. 4 , Article 1.
DOI: 10.6119/JMST-013-0313-2
Available at: https://jmstt.ntou.edu.tw/journal/vol22/iss4/1

This Research Article is brought to you for free and open access by Journal of Marine Science and Technology. It has been accepted for inclusion in Journal of Marine Science and Technology by an authorized editor of Journal of Marine Science and Technology.

Journal of Marine Science and Technology, Vol. 22, No. 4, pp. 405-416 (2014)
DOI: 10.6119/JMST-013-0313-2

ADDED MASS COMPUTATION FOR CONTROL OF AN OPEN-FRAME REMOTELY-OPERATED VEHICLE: APPLICATION USING WAMIT AND MATLAB

You-Hong Eng[1], Cheng-Siong Chin[2], and Michael Wai-Shing Lau[3]

Key words: modeling, simulation, remotely-operated vehicle, added mass, WAMIT™, MATLAB™.

ABSTRACT

In this paper, numerical modeling and testing of a complex-shaped remotely-operated vehicle (ROV) are shown. The paper emphasizes on systematic modeling of hydrodynamic added mass using computational fluid dynamic software WAMIT™ on the open frame ROV that is not commonly applied in practice. From initial design and prototype testing, a small-scale test using a free-decaying experiment is used to verify the theoretical models obtained from WAMIT™. Simulation results have shown to coincide with the experimental tests. The proposed method is able to determine the hydrodynamic added mass coefficients of the open frame ROV.

I. INTRODUCTION

Mathematical modeling and simulation are the heart of most current technological innovations and have become a fundamental tool in many fields of engineering. Essentially a multi-disciplinary in its applications, mathematical modeling and simulation are a key technology that have increased its presence within industries and institutions over the years. The proposed works on a marine vehicle such as an underwater robotic vehicle (URV) reflect this multidisciplinary system. In the last four decades, the applications of this multidisciplinary URV [1-3, 7-10, 12, 13] design has experienced tremendous growth. Many are used for underwater inspection of sub-sea cables, oil and gas installations like Christmas trees, structures and pipelines. They are essential at depths where the use of human divers is impractical. Based on the tasks and modes of operations, engineers and researchers have broadly classified the URV as remotely operated vehicle (ROV) and autonomous underwater vehicle (AUV). Nevertheless, ROV are suitable for works that involves operating from a stationary point or cruising at relatively slow speeds during pipeline inspection. For any tasks involving manipulation and requiring maneuverability, they are the most cost-effective platform.

However, to design the control system for the ROV, the dynamics of the vehicle need to be modeled and simulated. In the modeling process, the added mass coefficients are found to be difficult to obtain as the ROV is nonlinear in dynamics and asymmetry in design as compared to its counterpart, AUV, that is more streamlined. To circumvent this, the vehicle dynamics are often obtained using different test equipment. Most of the dynamic testing is conducted with the model undergoing forced lateral or vertical plane motions to determine the added masses, and other derivatives. Routine dynamic testing was introduced with the Planar Motion Mechanism (PMM) [11]. The PMM imparts harmonic oscillations to the model in order to determine the linear hydrodynamic coefficients while Marine Dynamic Test Facility [20] imparts large amplitude and high rate arbitrary motions to the model with six degrees of freedom (DOF) to measure the total forces and moments.

Although, the hydrodynamic added mass for the ROV are usually tested by these full-scale instrumented tow tank facilities, it could be difficult to justify building a facility for the ROV testing only. From initial design and prototype testing, a smaller scale testing is often desirable and economical to run during the developmental stage. With the advancement of computers, applications of computational-fluid dynamic (CFD) have evolved to a level of accuracy which allows them to apply to ships, and lately on the AUV [6, 18, 19, 21]. However, application on a complex bluff body with open frame structure like ROV is not readily available in the literature.

Paper submitted 10/29/12; revised 12/14/12; accepted 03/13/13. Author for correspondence: Cheng-Siong Chin (e-mail: cheng.chin@ncl.ac.uk).
[1] Acoustic Research Laboratory, Tropical Marine Science Institute, National University of Singapore, Singapore.
[2] School of Marine Science and Technology, Newcastle University, Newcastle upon Tyne, United Kingdom.
[3] School of Mechanical and Systems Engineering, Newcastle University, Newcastle upon Tyne, United Kingdom.

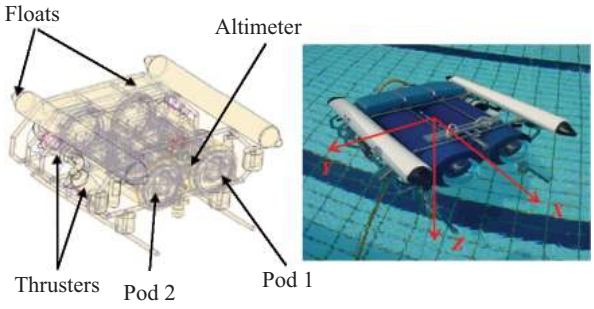

Fig. 1. Schematic of RRC ROV.

In this paper, a systematic approach of using Computer-aided design (CAD) software MULTISURF™ to mesh the ROV and the CFD software Wave Analysis MIT (WAMIT™) to determine the hydrodynamic added mass of the ROV is presented. All data generated during the computation are exported in ASCII format to different files. MATLAB™ [15] routines provide the capability to extract information from the data and generate the hydrodynamic added mass coefficients for the ROV. The simulated results are then compared with experimental study using a free-decaying scale model test [3] that is later translated into a full-scale model by the laws of Similitude. In summary, the proposed method provides a systematic approach to determine the hydrodynamic added mass coefficients of a complex-shaped ROV.

This paper is organized as follows: The dynamics model of the ROV is addressed in Section 2. In Section 3 the hydrodynamic added mass modeling process and comparisons with the empirical results are presented. In Section 4, the experimental results of the added mass coefficient using the free - decaying method is described. Lastly, the conclusion is drawn in Section 5.

II. ROV MODELING

Obtaining dynamic equations of the ROV is usually the first step in developing a simulation model. In this section, the basic design of the ROV is described. The initial test-bed ROV designed by Robotics Research Centre (RRC) [2] in Nanyang Technological University (NTU), RRC ROV (see Fig. 1) was tasked to perform underwater pipeline inspections such as locating pipe leakages or cracks. The twin "eyeball" ROV depicted in Fig. 1 has an open-frame structure and is 1 m long, 0.9 m wide, and 0.9 m high. It has a dry weight of 115 kg and a current operating depth of 100 m. Its designed tasks include inspections of underwater pipelines. The RRC ROV is underactuated as it has four thrusters inputs for only six degrees of freedom (DOFs) (that is surge, sway, heave, roll, pitch and yaw velocity) with a high degree of cross coupling between them. The roll and pitch motions are passive as the metacentric height is sufficient to provide adequate static stability. A brief description of the component layout of the RRC ROV is given.

Table 1. Notations used in ROV.

DOF	Motion Descriptions	Positions and Orientations	Linear and Angular Velocities
1	Motions in the x-direction (surge)	x	u
2	Motions in the y-direction (sway)	y	v
3	Motions in the z-direction (heave)	z	w
4	Rotations about the x-axis (roll)	ϕ	p
5	Rotations about the y-axis (pitch)	θ	q
6	Rotations about the z-axis (yaw)	ψ	r

- Four thrusters, each providing up to 70N of thrust;
- Two cylindrical floats with four balancing steel weight;
- Main pod (Pod 1) and sensors with navigational pod (Pod 2);
- Two halogen lamps and an altimeter.

After the preliminary design, the dynamics of the ROV need to be verified before the actual control system design process. Prior to ROV modeling, the following assumptions were made. There are namely:

- ROV is a rigid body and is fully submerged once in the water;
- Water is assumed to be ideal fluid that is incompressible, inviscid and irrotational;
- ROV is slow moving during pipeline inspection;
- The earth-fixed frame of reference is inertial;
- Disturbance due to wave is neglected as it is fully submerged;
- Tether dynamics attached to the ROV is not modeled.

The standard Society of Naval Architects and Marine Engineers (SNAME) notations used for the marine vehicle such as ROV are shown in Table 1.

Using the Newtonian approach, the motion of a rigid body with respect to the body-fixed reference frame at the origin (see Fig. 2) is given by the equation [8, 9]:

$$\mathbf{M_{RB}}\dot{\mathbf{v}} + \mathbf{C_{RB}}(\mathbf{v}) = \boldsymbol{\tau}_{\mathbf{RB}} \tag{1}$$

where $\mathbf{M_{RB}} \in \Re^{6\times6}$ is the mass-inertia matrix, $\mathbf{C_{RB}}(\mathbf{v}) \in \Re^{6\times6}$ is the Coriolis and centripetal matrix, $\boldsymbol{\tau}_{\mathbf{RB}} = [\boldsymbol{\tau}_{\mathbf{RB1}}\ \boldsymbol{\tau}_{\mathbf{RB2}}]^{\mathrm{T}} \in \Re^6$ is a vector of external forces and moments, $\mathbf{v} = [\mathbf{v_1}\ \mathbf{v_2}]^{\mathrm{T}} \in \Re^6$ is the linear and angular velocity vector namely: $\mathbf{v_1} = [u\ v\ w]^{\mathrm{T}}$ and $\mathbf{v_2} = [p\ q\ r]^{\mathrm{T}}$, respectively.

The mass inertia matrix given in (1) can be written as:

$$\mathbf{M_{RB}} = \begin{bmatrix} m & 0 & 0 & 0 & mz_G & -my_G \\ 0 & m & 0 & -mz_G & 0 & mx_G \\ 0 & 0 & m & my_G & -mx_G & 0 \\ 0 & -mz_G & my_G & I_x & -I_{xy} & -I_{xz} \\ mz_G & 0 & -mx_G & -I_{yx} & I_y & -I_{yz} \\ -my_G & mx_G & 0 & -I_{zx} & -I_{zy} & I_z \end{bmatrix} \tag{2}$$

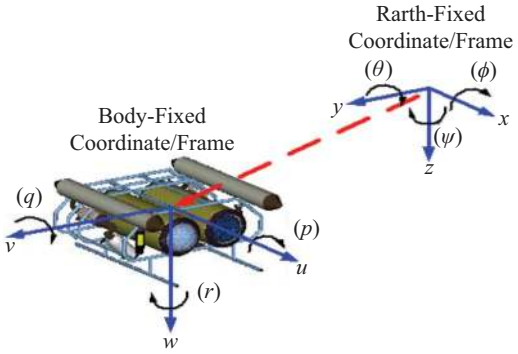

Fig. 2. Coordinate systems used in ROV.

where x_G, y_G, z_G are the coordinates of the center of gravity and m is the mass of the ROV. Here I_x, I_y, I_z are the moments of inertia about axes of the ROV, and $I_{xy} = I_{yx}$, $I_{xz} = I_{zx}$, $I_{yz} = I_{zy}$ are the products of inertia.

Similarly, the Coriolis and centripetal terms, describing the angular motion of the ROV can be expressed as:

$$\mathbf{C_{RB}}(\mathbf{v}) = \begin{bmatrix} \mathbf{0}_{3\times3} & \mathbf{C_{12}}(\mathbf{v}) \\ -\mathbf{C}_{12}^{\mathrm{T}}(\mathbf{v}) & \mathbf{C_{22}}(\mathbf{v}) \end{bmatrix} \tag{3}$$

with

$$\mathbf{C_{12}}(\mathbf{v}) = \begin{bmatrix} m(y_G q + z_G r) & -m(x_G q - w) & -m(x_G r + v) \\ -m(y_G p - w) & m(z_G r + x_G p) & -m(y_G r - u) \\ -m(z_G p - v) & -m(z_G q - u) & m(x_G p + y_G q) \end{bmatrix} \tag{4}$$

$$\mathbf{C_{22}}(\mathbf{v}) = \begin{bmatrix} 0 & -I_{yz}q - I_{xz}p + I_z r & I_{yz}r + I_{xy}p - I_y q \\ I_{yz}q + I_{xz}p - I_z r & 0 & -I_{xz}r - I_{xy}q + I_x p \\ -I_{yz}r - I_{xy}p + I_y q & I_{xz}r + I_{xy}q - I_x p & 0 \end{bmatrix} \tag{5}$$

The external force and moment vector $\boldsymbol{\tau}_{\mathbf{RB}}$ include the hydrodynamic forces and moments, $\boldsymbol{\tau}_{\mathbf{H}}$ due to damping, the restoring force and moment, and inertial of surrounding fluid known as added mass, and the propulsion inputs, $\boldsymbol{\tau}$. These forces and moments tend to oppose the motion of the ROV. The restoring forces and moments are dependent on the velocities and accelerations of the vehicle. They are therefore expressed in the body-fixed frame. The open-loop nonlinear ROV dynamic equations can be expressed as follows.

$$\mathbf{M}\dot{\mathbf{v}} + \mathbf{C}(\mathbf{v})\mathbf{v} + \mathbf{D}(\mathbf{v})\mathbf{v} + \mathbf{G_f}(\boldsymbol{\eta}) = \boldsymbol{\tau} \tag{6}$$

where $\mathbf{v} = [\mathbf{v_1} \quad \mathbf{v_2}]^{\mathrm{T}} = [u \quad v \quad w \quad p \quad q \quad r]^{\mathrm{T}}$ is the body-fixed velocity vector and $\boldsymbol{\eta} = [\boldsymbol{\eta_1} \quad \boldsymbol{\eta_2}]^{\mathrm{T}}$ is the earth-fixed vector, comprising the position vector $\boldsymbol{\eta_1} = [x \; y \; z]^{\mathrm{T}}$ and the orientation vector of Euler angles, $\boldsymbol{\eta_2} = [\phi \quad \theta \quad \psi]^{\mathrm{T}}$. $\mathbf{M} = \mathbf{M_{RB}} + \mathbf{M_A} \in \Re^{6\times6}$ is the sum of the rigid body inertia mass and added fluid inertia mass matrix, $\mathbf{C}(\mathbf{v}) = \mathbf{C_{RB}}(\mathbf{v}) + \mathbf{C_A}(\mathbf{v}) \in \Re^{6\times6}$ is the sum of Coriolis and centripetal and the added mass forces and moments matrix, $\mathbf{D}(\mathbf{v}) \in \Re^{6\times6}$ is the damping matrix due to the surrounding fluid, and $\mathbf{G_f}(\boldsymbol{\eta}) \in \Re^6$ is the gravitational and buoyancy vector. The propulsion forces and moments vector $\boldsymbol{\tau} = \mathbf{T}\bar{\mathbf{u}} \in \Re^6$ relates the thrust output vector $\mathbf{u} = \mathbf{F_T}\bar{\mathbf{u}} \in \Re^4$ with the thruster configuration matrix $\mathbf{T} \in \Re^{6\times4}$, $\mathbf{F_T} \in \Re^{4\times4}$ is the dynamics of each thruster and converts the input voltage command $\bar{\mathbf{u}} \in \Re^4$ into thrusts to propel the vehicle.

As shown in (6), the motion of the surrounding body of fluid in response to the ROV motion manifests itself as the hydrodynamic forces and moments resist the vehicle motion. The effect appears to be like "added" mass and inertia. For a fully submerged vehicle, the added mass and inertia are independent of the wave circular frequency. The added mass coefficients are expressed as follows:

$$\mathbf{M_A} = \begin{bmatrix} X_{\dot{u}} & X_{\dot{v}} & X_{\dot{w}} & X_{\dot{p}} & X_{\dot{q}} & X_{\dot{r}} \\ Y_{\dot{u}} & Y_{\dot{v}} & Y_{\dot{w}} & Y_{\dot{p}} & Y_{\dot{q}} & Y_{\dot{r}} \\ Z_{\dot{u}} & Z_{\dot{v}} & Z_{\dot{w}} & Z_{\dot{p}} & Z_{\dot{q}} & Z_{\dot{r}} \\ K_{\dot{u}} & K_{\dot{v}} & K_{\dot{w}} & K_{\dot{p}} & K_{\dot{q}} & K_{\dot{r}} \\ M_{\dot{u}} & M_{\dot{v}} & M_{\dot{w}} & M_{\dot{p}} & M_{\dot{q}} & M_{\dot{r}} \\ N_{\dot{u}} & N_{\dot{v}} & N_{\dot{w}} & N_{\dot{p}} & N_{\dot{q}} & N_{\dot{r}} \end{bmatrix} \tag{7}$$

where $X_{\dot{u}}$ is the added mass along X-axis due to an acceleration $\dot{u}$ in X-direction, $X_{\dot{v}}$ is the added mass along X-axis due to an acceleration $\dot{v}$ in Y-direction and so forth.

The hydrodynamic added Coriolis and centripetal matrix that consists of the added mass coefficients in (7) is given by:

$$\mathbf{C_A}(\mathbf{v}) = \begin{bmatrix} 0 & 0 & 0 & 0 & -a_3 & a_2 \\ 0 & 0 & 0 & a_3 & 0 & -a_1 \\ 0 & 0 & 0 & -a_2 & a_1 & 0 \\ 0 & -a_3 & a_2 & 0 & -b_3 & b_2 \\ a_3 & 0 & -a_1 & b_3 & 0 & -b_1 \\ -a_2 & a_1 & 0 & -b_2 & b_1 & 0 \end{bmatrix} \tag{8}$$

where

$$\begin{aligned} a_1 &= X_{\dot{u}}u + X_{\dot{v}}v + X_{\dot{w}}w + X_{\dot{p}}p + X_{\dot{q}}q + X_{\dot{r}}r \\ a_2 &= X_{\dot{v}}u + Y_{\dot{v}}v + Y_{\dot{w}}w + Y_{\dot{p}}p + Y_{\dot{q}}q + Y_{\dot{r}}r \\ a_3 &= X_{\dot{w}}u + Y_{\dot{w}}v + Z_{\dot{w}}w + Z_{\dot{p}}p + Z_{\dot{q}}q + Z_{\dot{r}}r \\ b_1 &= X_{\dot{p}}u + Y_{\dot{p}}v + Z_{\dot{p}}w + K_{\dot{p}}p + K_{\dot{q}}q + K_{\dot{r}}r \\ b_2 &= X_{\dot{q}}u + Y_{\dot{q}}v + Z_{\dot{q}}w + K_{\dot{q}}p + M_{\dot{q}}q + M_{\dot{r}}r \\ b_3 &= X_{\dot{r}}u + Y_{\dot{r}}v + Z_{\dot{r}}w + K_{\dot{r}}p + M_{\dot{r}}q + N_{\dot{r}}r \end{aligned} \tag{9}$$

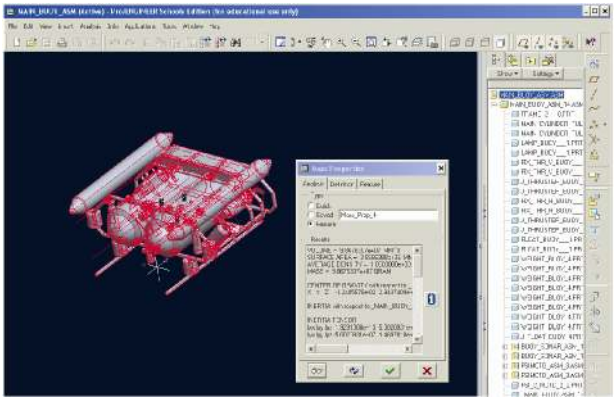

Fig. 3. CAD software PRO/ENGINEER™ for ROV.

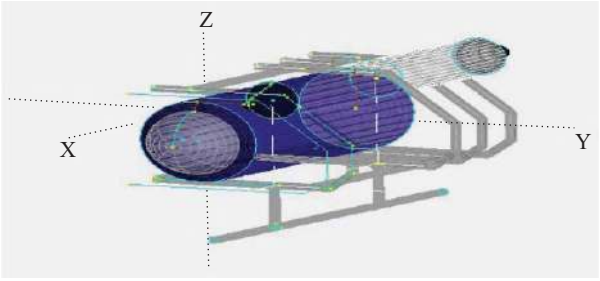

Fig. 4. Finite surface panels generation [4] using MULTISURF™.

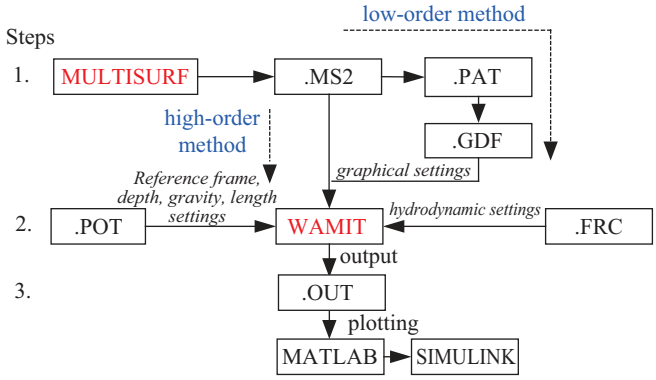

Fig. 5. Overall programs flowchart for computing added mass coefficients.

III. HYDRODYNAMIC ADDED MASS MODEL

In this section, the steps involving in determining the added mass coefficients of the ROV are described. Most of the works on hydrodynamic added mass modeling and testing were performed and documented in the report [4] and paper [5]. The CAD software PRO/ENGINEER™ (see Fig. 3) was used to determine the rigid-body mass and inertia of the ROV. The principal components were included in the complete ROV geometric model using the density, the rigid-body mass and inertia properties with respect to the ROV's center of gravity.

By adding balancing weights at a designated location on the ROV, the location of the center of gravity was made to coincide with the ROV origin. The parameters used in (2) become:

$$m = 115.00 \text{ kg}, I_x = 6.1000 \text{ kg.m}^2, I_y = 5.9800 \text{ kg.m}^2,$$

$$I_{xz} = -0.1850 \text{ kg.m}^2, I_{yz} = 0.0006 \text{ kg.m}^2,$$

$$I_z = 5.5170 \text{ kg.m}^2, I_{xy} = -0.0002 \text{ kg.m}^2.$$

After the mass and the inertia matrix were obtained, the 3D geometric model in Fig. 3 was converted into finite surface panels using MULTISURF™ in Fig. 4.

The geometry from MULTISURF™ was then imported to WAMIT™ using the high-order panel method. The output from the WAMIT™ was plotted using the MATLAB™ and Simulink™ software. The following chart in Fig. 5 shows how the three programs, namely MATLAB™, MULTISURF™, and WAMIT™ are used together in the hydrodynamic added mass analysis.

The important parameters that are specified in the files are shown in Figs. 6 to 8. These files are meant for the study of the sphere which will be modified for the ROV. As seen in Fig. 6, the first line provides a brief description of the file. Height of water column from bottom (HBOT) is the dimensional water depth where '-1' indicates infinite water depth. X-dimension of body (XBODY) is the dimensional coordinates of the origin of the body-fixed coordinate system. As seen in Fig. 7, it specifies the hydrodynamics output from the WAMIT™. As shown in Fig. 8, Undimensioned length (ULEN) is the dimensional length characterizing the body dimension and it has a value of one. Gravitational acceleration (GRAV) is 9.80665 m/s^2. The four consecutive lines are the x-y-z coordinates of a panel specified by four points. Other parameters used in the files can be found and explained in the WAMIT™ user manual [14]. The MATLAB™ script was used to display and plot the added mass results.

Prior to the application of the WAMIT™ to the ROV [4, 5], a few studies on the empirical results of a sphere and a cylinder were performed to verify the program setup and parameters. In higher-order method, size of different panels is used to represent different shapes, hence allowing different number of panels to represent a surface individually. However, the iterative method for the solution of the linear system may fail to converge in many cases. A direct or block-iterative solution options are recommended in these cases. And with geometry that has sharp corners, the result can be less accurate.

To improve the accuracy and consistency of the results, the body of interests (that is the ROV) is divided into parts and solved incrementally. Since the ROV is made up of simple geometrical shapes such as sphere and cylinder (see Fig. 1), the empirical results of the added mass of simple geometry bodies such as the sphere and cylinder were used. Studies had been conducted to verify the results from WAMIT™ are

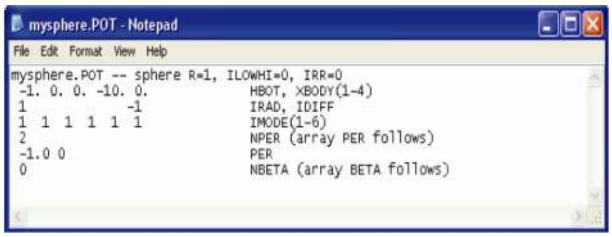

Fig. 6. Potential Control File (POT) [4].

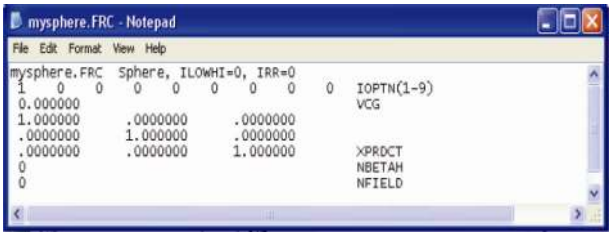

Fig. 7. FRC (Force Control File) [4].

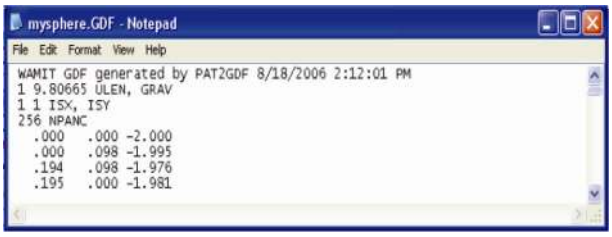

Fig. 8. GDF (Geometry Data File) [4].

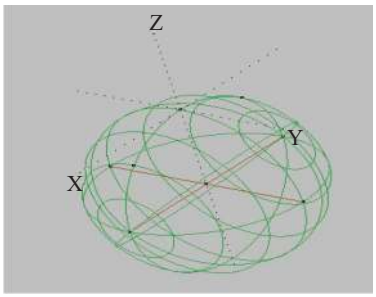

Fig. 9. Sphere drawn in MULITSURF [4] [origin = (0, 0, 0), radius r = 1 m, density ρ = 1].

similar to the empirical results. For example, the theoretical added mass of a sphere (see Fig. 9) is $2/3\pi\rho r^3$ for surge, sway and heave direction. By normalizing the mass against the density, ρ, the added mass of the sphere becomes $2/3\pi r^3$.

As shown in Table 2, the results obtained from WAMIT^{TM} are within 0.5% of the theoretical results using the lower order method. On the other hand, the results using the higher order method have no error. In cylinder case (see Fig. 10), the results from WAMIT^{TM} are within 1.4% of the theoretical results shown in Table 3. The results using high-order method are more accurate and converged faster than the lower order

Table 2a. Low-order method for sphere [4].

Panel Number	Low-Order Method					
	Theoretical			Numerical		
	Surge	Sway	Heave	Surge	Sway	Heave
256	2.0944	2.0944	2.0944	2.0171	2.0892	2.0892
512				2.0183	2.0972	2.0929
1024				2.0749	2.0929	2.0929
2304				2.0861	2.0939	2.0940
			Total	-0.4%	-0.01%	~0%

Table 2b. High-order method for sphere [4].

Panel Number	High-Order Method					
	Theoretical			Numerical		
	Surge	Sway	Heave	Surge	Sway	Heave
256	2.0944	2.0944	2.0944	2.0952	2.0919	2.0924
512				2.0944	2.0944	2.0945
1024				2.0944	2.0944	2.0945
2304				2.0944	2.0944	2.0945
			Total	0%	0%	0%

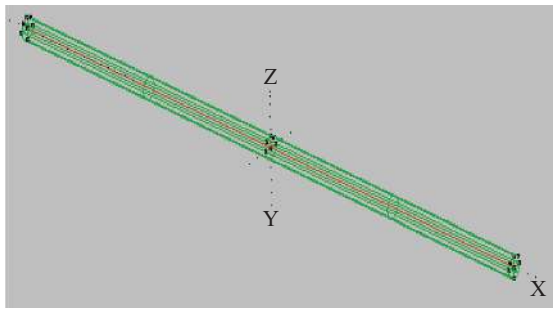

Fig. 10. Cylinder drawn [4] in MULTISURF^{TM} [Origin = (0, 0, 0), radius = 1 m, length = 80 m].

method. One of the most important issues in computational fluid dynamics is the convergence of the result. As the body of interests is divided into small parts and solved individually, the results should converge as higher numbers of elements or panels are used. As observed in both Tables 2 and 3, the calculated added mass converges to the theoretical value as the number of panels increased.

In WAMIT^{TM}, the depth of the submerged body needs to be specified. The same sphere was used to study the effects of the depth on the added mass. The theoretical added mass of the sphere in the X direction is 2.9044. The added mass results of the sphere converge at 10 m as seen in Table 4. With that, the subsequent added mass analysis on the ROV was performed at this water depth.

Another concern on the CFD using WAMIT^{TM}, is the result can be inaccurate when processing a geometry that has sharp corners and large number of geometry. To circumvent this,

Table 3a. Low-order method for cylinder [4].

Panel Number	Low-Order Method			
	Theoretical		Numerical	
	Surge	Heave	Sway	Heave
768	251.3274	251.3274	249.6437 (-0.7%)	249.8821 (-0.6%)
3072			248.0583 (-1.3%)	248.2957 (-1.2%)

Table 3b. High-order method for cylinder [4].

Panel Number (Panel number)	High-Order Method			
	Theoretical		Numerical	
	Surge	Heave	Sway	Heave
5 (75)	251.3274	251.3274	247.6803	247.7656
2 (150)			247.4787	247.5613
1 (368)			247.4198	247.5017
		Total	-1.4%	-1.4%

Table 4. Added mass of sphere at various depths [4].

Depth (m)	Added Mass (Kg)
0	2.5910
1	2.1419
2	2.1073
5	2.0947
10	2.0931
100	2.0929

only half of the ROV was modeled due to its symmetry in the XZ plane. As shown in Fig. 4, the main components of the ROV were drawn to reduce the complexity in the computation. In this paper, the thrusters were omitted in the computation. This can be verified by the results in Tables 5a and 5b. The diagonal components of the added mass for the case of two (T2) and four thrusters (T4) are small, as compared to the ROV without thrusters (see Fig. 11 on the left-hand side). In addition, the added coefficients of the thruster are indeed quite small ($\approx 10^{-3}$) as seen in (10).

$$-\begin{bmatrix} 0.00019 & 0 & 0 & 0 & 0 & 0 \\ 0 & 0.0009 & 0 & 0 & 0 & 0.00004 \\ 0 & 0 & 0.0009 & 0 & 0.00004 & 0 \\ 0 & 0 & 0 & 0 & 0 & 0 \\ 0 & 0 & 0.00004 & 0 & 0.000004 & 0 \\ 0 & 0.00004 & 0 & 0 & 0 & 0.000004 \end{bmatrix} \quad (10)$$

As a result, the thrusters' contribution on the added mass matrix can be ignored.

Table 5a. Magnitude of error on diagonal components of added mass matrix (Column 1 to 3) (T2-two thrusters and T4-four thrusters).

M_A	Col 1		Col 2		Col 3	
	T2	**T4**	T2	**T4**	T2	**T4**
Row 1	-0.03	**0.03**	0	**0**	10	**72**
Row 2	0	**0**	0.003	**0**	0	**0**
Row 3	1	**-7**	0	**0**	0.02	**0.06**
Row 4	0	**0**	2	**2**	0	**0**
Row 5	-4	**-2**	0	**0**	-34	**-38**
Row 6	0	**0**	-28	**-28**	0	**0**

Table 5b. Magnitude of error on diagonal components of added mass matrix (Column 4 to 6) (T2-two thrusters and T4-four thrusters)

M_A	Col 4		Col 5		Col 6	
	T2	**T4**	T2	**T4**	T2	**T4**
Row 1	0	**0**	-4	**-6**	0	**0**
Row 2	2	**2**	0	**0**	-28	**-28**
Row 3	0	**0**	-32	**-34**	0	**0**
Row 4	0.07	**0.1**	0	**0**	32	**33**
Row 5	0	**0**	-1.7	**-2**	0	**0**
Row 6	27	**29**	0	**0**	-1	**-1**

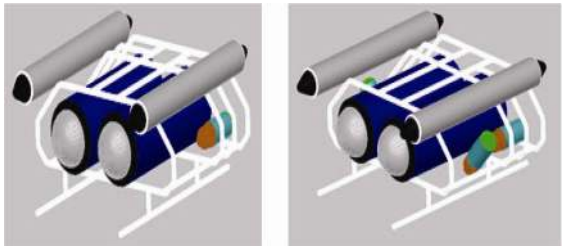

Fig. 11. ROV model drawn in MULTISURF™ (with two and four thrusters) [4].

During the modeling of the components, various locations and orientation of the reference frame were defined. To verify whether the effects of these reference frames can affect the added mass coefficients, Table 6 shows the effects of changing the orientation and location of the reference plane in the CAD model. It was found that the changes were not significant as compared to the diagonal element of the added mass matrix.

In the subsequent section, a scale model of the ROV was used to obtain the experimental results of the added mass coefficients. To facilitate the study of the scale ROV model, the results of the scale ROV was compared with the actual ROV. It was found that the scale model can shape by a factor R expressed in a matrix form as seen in the last column of Table 7. By doing so, each element in the added mass matrix is scaled to obtain the actual results.

Table 7. Scaling apply to full scale model [4].

Scale	Added Mass Matrix	Matrix (to apply on scale model)
Full-Scale (original)	$-\begin{bmatrix} 21.1403 & 0 & 0.0619 & 0 & -0.5748 & 0 \\ 0 & 51.7012 & 0 & -2.0928 & 0 & -0.3767 \\ 0.0917 & 0 & 92.4510 & 0 & 0.5871 & 0 \\ 0 & -2.0090 & 0 & 3.6191 & 0 & 0.0235 \\ -0.5237 & 0 & 0.5594 & 0 & 2.6427 & 0 \\ 0 & -0.3783 & 0 & 0.0275 & 0 & 2.3033 \end{bmatrix}$	
Half-Scale (R = 2)	$-\begin{bmatrix} 2.6425 & 0 & 0 & 0.0077 & -0.0359 & 0 \\ 0 & 6.4626 & 0 & -0.1308 & 0 & -0.0235 \\ 0.0115 & 0 & 11.5562 & 0 & 0.0367 & 0 \\ 0 & -0.1256 & 0 & 0.1131 & 0 & 0.0007 \\ -0.0327 & 0 & 0.0350 & 0 & 0.0826 & 0 \\ 0 & -0.0236 & 0 & 0.0009 & 0 & 0.0720 \end{bmatrix}$	$\left[\begin{array}{ccc\|ccc} R^3 & 0 & R^3 & 0 & R^4 & 0 \\ 0 & R^3 & 0 & R^4 & 0 & R^4 \\ R^3 & 0 & R^3 & 0 & R^4 & 0 \\ \hline 0 & R^4 & 0 & R^5 & 0 & R^5 \\ R^4 & 0 & R^4 & 0 & R^5 & 0 \\ 0 & R^4 & 0 & R^5 & 0 & R^5 \end{array}\right]$
Ouarter-Scale (R = 4)	$-\begin{bmatrix} 0.3303 & 0 & 0.0010 & 0 & -0.0022 & 0 \\ 0 & 0.8078 & 0 & -0.0082 & 0 & -0.0015 \\ 0.0014 & 0 & 1.4445 & 0 & 0.0023 & 0 \\ 0 & -0.0078 & 0 & 0.0035 & 0 & 0 \\ -0.0020 & 0 & 0.0022 & 0 & 0.0026 & 0 \\ 0 & -0.0015 & 0 & 0 & 0 & 0.0022 \end{bmatrix}$	$\left[\begin{array}{ccc\|ccc} R^3 & 0 & R^3 & 0 & R^4 & 0 \\ 0 & R^3 & 0 & R^4 & 0 & R^4 \\ R^3 & 0 & R^3 & 0 & R^4 & 0 \\ \hline 0 & R^4 & 0 & R^5 & 0 & R^5 \\ R^4 & 0 & R^4 & 0 & R^5 & 0 \\ 0 & R^4 & 0 & R^5 & 0 & R^5 \end{array}\right]$

Table 6. Effects of the changes in added mass matrix [4].

Items	Case Studies	Results
1	Effect of changing origin of the reference frame	No changes in the added mass coefficients in translation directions. Some changes in the rotational directions and the off-diagonal terms of the added mass matrix.
2	Effect of changing orientation of the reference frame	No changes in the added mass matrix.

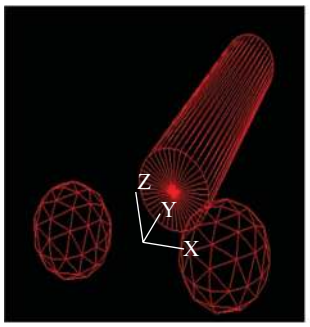

AMASS 3D JAVA Applet

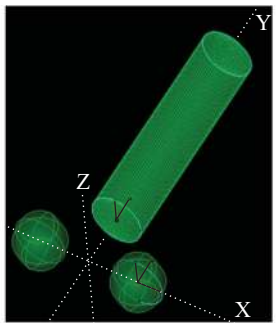

WAMIT-MULTISURF™

26.1799	0.0	0.0	0.0	0.0	-150.7964
0.0	5.236	0.0	0.0	0.0	0.0
0.0	0.0	26.1799	150.7964	0.0	0.0
0.0	0.0	150.7964	1038.82	0.0	0.0
0.0	0.0	0.0	0.0	4.1888	0.0
-150.7964	0.0	0.0	0.0	0.0	1043.0085

25.6599	0.0000	-0.0000	-0.0000	-0.0035	-128.3408
-0.0000	7.7120	0.0013	0.0318	-0.0000	0.0000
-0.0000	0.0013	26.4639	130.1422	-0.0000	0.0000
-0.0000	0.0317	130.1423	857.2991	0.0000	0.0000
-0.0034	-0.0000	-0.0000	0.0000	16.3677	0.0144
-128.3457	0.0000	0.0000	-0.0000	0.0151	866.8915

Fig. 12. Comparisons of methods to obtain added mass coefficients (see the matrix below pictures) [4].

As observed in the ROV design, it has more than one component in the body design. The effects of the multi-bodies such as two spheres and a cylinder were analyzed. The multiple bodies in MULTISURF™ could be drawn simultaneously for analysis in WAMIT™. The mesh of these multi-bodies was created in MULTISURF™ and later using WAMIT™ to compute the added mass matrix. The results were compared with the Java Amass applet (that was constructed for the usage of Marine Hydrodynamics students in MIT). The JAVA Amass applet was used to approximate the added mass of various objects composed by spheres and cylinders. A comparison between the added mass calculated by the two methods is shown in Fig. 12. The location of zero elements in both added mass matrix is identical. Even though the value of non-zero elements could not match exactly, the maximum deviation is less than 20%. Hence, the steps involved using WAMIT™ to determine the added mass coefficients of the ROV are performed correctly.

The WAMIT™ solved the ROV over finite panels using the higher-order panel method. The convergences of the solution are shown in Fig. 13(a) and 13(b). As observed, the added mass values settle to the desired values at around 500-1000 unknowns or panels in the linear system. The computed added mass parameters give a positive definite matrix. All the eigenvalues (that is equal to 21.1403, 51.7012, 92.4510, 3.6191, 2.6427, 2.3033) of the added mass matrix are greater than zero. Besides, the data indicate that the added mass is smallest in the surge DOF and largest in the heave DOF. This is consistent

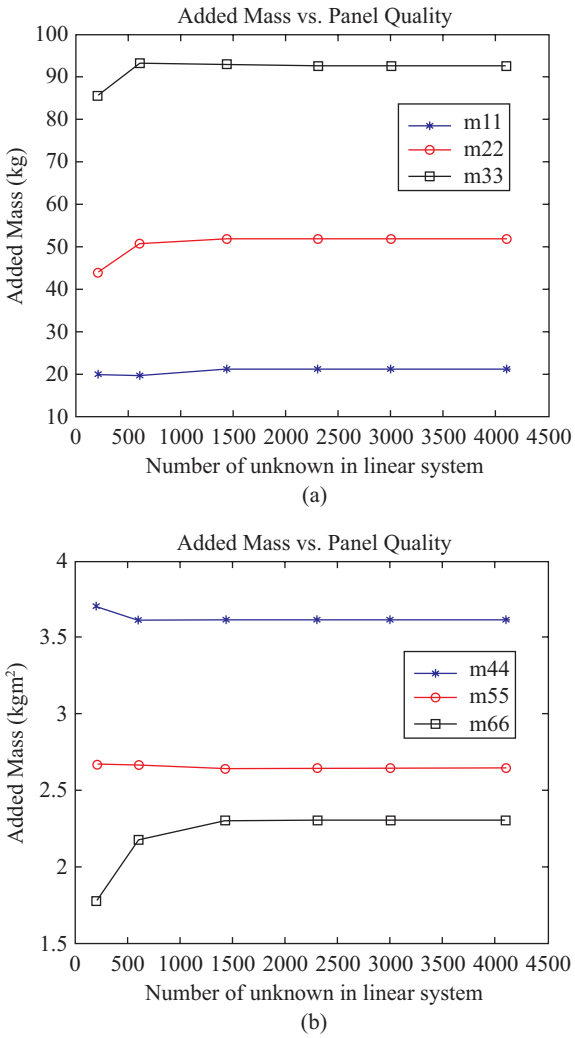

Fig. 13. (a) Convergence test for added mass of RRC ROV [4]. (b) Convergence test for the remaining added mass of RRC ROV [4].

with the fact that ROV's cross-section area is smaller in the surge DOF and largest in heave DOF.

In summary, the final added mass matrix of the RRC ROV becomes:

$$\mathbf{M}_A = -\begin{bmatrix} 21.1403 & 0 & 0.0619 & 0 & -0.5748 & 0 \\ 0 & 51.7012 & 0 & -2.0928 & 0 & -0.3767 \\ 0.0917 & 0 & 92.4510 & 0 & 0.5871 & 0 \\ 0 & -2.0090 & 0 & 3.6191 & 0 & 0.0235 \\ -0.5237 & 0 & 0.5594 & 0 & 2.6427 & 0 \\ 0 & -0.3783 & 0 & 0.0275 & 0 & 2.3033 \end{bmatrix} \tag{11}$$

The negative signs present in (11) arise as the pressure forces on the ROV would tend to retard the vehicle motion. The real mass (or the rigid body mass) and the virtual added mass are originally on opposite sides of the equation; one is a rigid body property, while the other is related to the force experienced by the vehicle when the virtual mass is "subtracted" from the real mass. The net effect has a greater apparent mass in most DOF.

As observed, the off-diagonal terms in $\mathbf{M}_A$ are smaller as compared to its diagonal components $\mathbf{M}_A$. For lower speed underwater vehicles, the off-diagonal terms are often neglected [8]. This approximation is found to hold true for many applications. Hence, $\mathbf{M}_A$ is simplified as shown.

$$\mathbf{M}_A = -\begin{bmatrix} 21.1403 & 0 & 0 & 0 & 0 & 0 \\ 0 & 51.7012 & 0 & 0 & 0 & 0 \\ 0 & 0 & 92.4510 & 0 & 0 & 0 \\ 0 & 0 & 0 & 3.6191 & 0 & 0 \\ 0 & 0 & 0 & 0 & 2.6427 & 0 \\ 0 & 0 & 0 & 0 & 0 & 2.3033 \end{bmatrix} \tag{12}$$

where the corresponding Coriolis/centripetal added mass matrix in (8) becomes:

$$\mathbf{C}_A(\mathbf{v}) = \begin{bmatrix} 0 & 0 & 0 & 0 & -92.4510w & 51.7012v \\ 0 & 0 & 0 & 92.4510w & 0 & -21.1403u \\ 0 & 0 & 0 & -51.7012v & 21.1403u & 0 \\ 0 & -92.4510w & 51.7012v & 0 & -2.3033r & 2.6427q \\ 92.4510w & 0 & -21.1403u & 2.3033r & 0 & -3.6191p \\ -51.7012v & 21.1403u & 0 & -2.6427q & 3.6191p & 0 \end{bmatrix} \tag{13}$$

In summary, the added mass matrix for the ROV has been determined using WAMIT™ based on the potential flow theory and panel method. The added mass for surge, sway and heave motion is approximately 21 kg, 51 kg and 93 kg, respectively. After considering the added mass, the effective inertia for ROV in heave motion increased from 115 kg to 208 kg. This implies that the added mass forces are quite significant and cannot be neglected in the ROV dynamics model.

IV. EXPERIMENTAL RESULTS OF ADDED MASS COEFFICIENT USING FREE-DECAYING METHOD

In the previous sections, the parameters associated with the hydrodynamic added mass on the ROV were estimated using WAMIT™. Most of the works on hydrodynamic added mass testing were performed and documented [4, 5]. However, based on CFD guidelines [22] these parameter values should be corroborated by other means. The accuracy of the results can only be truly determined if the results can be independently confirmed using different approaches. Therefore, in this section, the added mass parameters was verified by comparing the value predicted by CFD using the scale model of the ROV.

By applying the laws of Similitude, the hydrodynamics parameters of the scale model can be scale up to predict the corresponding values for the actual ROV model. The free-decaying test is designed for a small class of complex

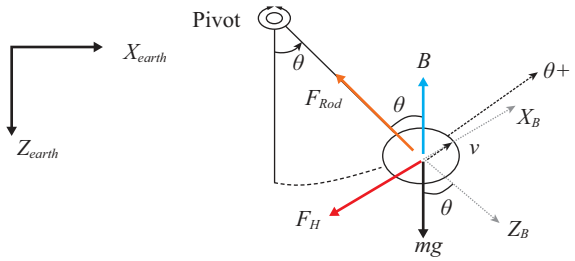

Fig. 14. Free body diagram of the setup [4].

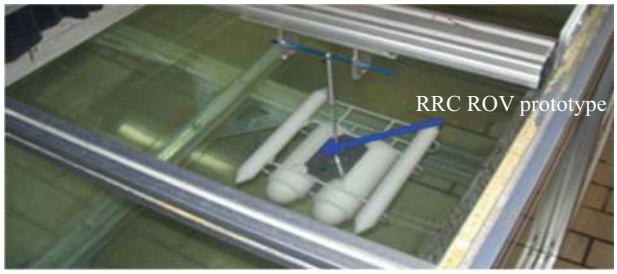

Fig. 15. RRC ROV prototype in water tank (orientated in surge direction) [4].

Fig. 16. Image Sequence of the scale model under pendulum motion- in surge direction [4].

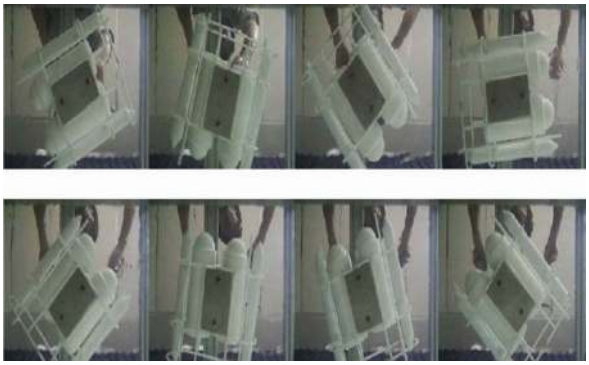

Fig. 17. Image sequence of the scale model in the yaw direction [4].

bluff underwater vehicle such as the RRC ROV. The hydrodynamics added mass parameters can be extracted from an experiment as shown in Fig. 14, in which the scale model was attached to the end of the rod. The rod will perform a free decay motion in water. The least-square approach was then applied to determine the hydrodynamic added mass parameters [1, 4, 5].

To perform the experiments according to the concept shown in Fig. 14, experiments were carried out in a 0.3 m × 0.2 m × 0.3 m open tank (see Fig. 15) giving a characteristics length ratio of about 0.3:1 for the ROV to investigate the motion characteristics of the scale ROV in surge, sway, heave, and yaw in the positive direction. The scale ROV model was attached to the end of a pendulum and submerged in water held by an aluminum frame mounted at the edges of the water tank. The pendulum was set in motion. With a small black mark on the rod, the motion of the pendulum was captured by a video camera. The recorded trajectory of the black mark was digitised using an open-source program VirtualDubMod [16]. For each frame, the X and Y coordinates of the black mark were acquired for image processing using MATLAB™ Image Processing Toolbox. The video was split into multiple frames up to 30 frames per second. Figs. 16 and 17 show some image frames of the free decay motion of the pendulum in both the surge and yaw direction. In the earth-fixed frame, the scale model is constrained to rotate in a single plane about the pivot point.

A similar test in the heave direction, with the scale model rotated 90° facing the direction of the motion, was performed to estimate the parameters in yaw direction. In order to identify the parameters in the yaw motion, the pendulum rod was replaced by a torsion spring. The image sequence of the scale model in the yaw direction is shown in Fig. 17. The scale model exhibits a pure rotational motion in water.

Each experiment was repeated a few times for different velocity. The average added mass readings (e.g. longitudinal force, transverse force, attitudinal force and moment) were obtained. As a result, the curves for the thrust versus the motion variables u, v, w, and r were obtained. With the vehicle surge, sway or heave set to a constant velocity, the thrust can be considered to be equal to the hydrodynamic force. The moments can be considered to be equal to the hydrodynamic moments when it yaws at a constant angular velocity. Therefore, the curves of the thrust versus the motion variables are assumed to be similar to the curves of hydrodynamic loads. As the hydrodynamic forces resist the motion, the amplitude of the swing will decay slowly over time as seen in Figs. 18(a) to 18(c). The hydrodynamics added mass coefficients were determined offline using the least-square method.

In the experiment, the amplitude of the wave created by the ROV is smaller than the amplitude created by the pendulum itself. As seen in Tables 8a to 8d, the changes in the velocity (i.e. the speed of the free-decaying test) do not significantly affect the hydrodynamic parameters. Hence, the test regime is still within the “steady-state” with a little wave contributed by the scale ROV at a low speed of 0.55 m/s (maximum). Based

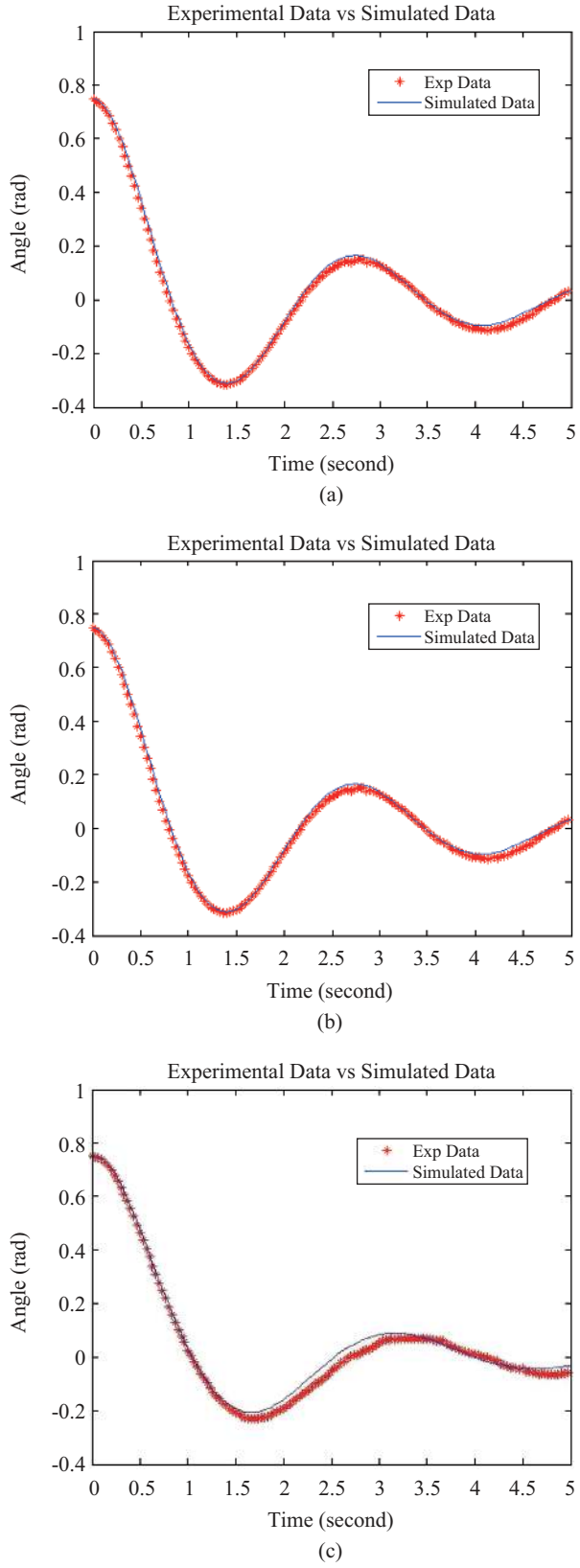

Fig. 18. (a) Experiment data versus simulated data in surge direction [4], (b) Experiment data versus simulated data in heave direction [4], and (c) Experiment data versus simulated data in yaw direction [4].

Table 8a. Hydrodynamic parameters at different velocity (surge direction) [4].

Direction	Max. Speed	Added Mass coefficient	RMS error
Surge	**0.55 m/s***	**0.5581**	**0.0568**
		0.6054	**0.0500**
		0.5765 (Avg: 0.580)	**0.0552**
	0.50 m/s	0.5134	0.0572
		0.5011	0.0685
		0.5125	0.0717
	0.35 m/s	0.3541	0.0632
		0.4078	0.0541
		0.4109	0.0797

Table 8b. Hydrodynamic parameters at different velocity (sway direction) [4].

Direction	Max. Speed	Added Mass coefficient	RMS error
Sway	0.55 m/s	1.5491	0.0266
		1.5578	0.0372
		1.5713	0.0213
	0.50 m/s*	**1.4347**	**0.0277**
		1.5465	**0.0234**
		1.4878 (Avg: 1.489)	**0.0269**
	0.35 m/s	1.2735	0.0294
		1.1198	0.0333
		1.1899	0.0459

Table 8c. Hydrodynamic parameters at different velocity (heave direction) [4].

Direction	Max. Speed	Added Mass coefficient	RMS error
Heave	0.55 m/s	5.4789	0.0240
		4.9989	0.0331
		5.0811	0.0423
	0.50 m/s	4.9976	0.0341
		4.8126	0.0556
		4.7894	0.0421
	0.35 m/s*	**3.0760**	**0.0239**
		3.1407	**0.0219**
		2.9909 (Avg: 3.069)	**0.0277**

Table 8d. Hydrodynamic parameters at different velocity (for yaw direction) [4]

Direction	Max. Speed	Added Mass coefficient	RMS error
Yaw	0.35 rad/s	0.0037	0.0311
		0.0023	0.0425
		0.0029	0.0511
	0.50 rad/s	0.0037	0.0427
		0.0043	0.0588
		0.0057	0.0403
	0.55 rad/s*	**0.0065**	**0.0320**
		0.0090	**0.0300**
		0.0110 (Avg: 0.008)	**0.0380**

Table 9. Added mass coefficients obtained [4] from free decay experiment and WAMIT™.

Methods	Added Mass Coefficients			
	Surge (0-0.55 m/s)	Sway (0-0.55 m/s)	Heave (0-0.55 m/s)	Yaw (0-0.55 rad/s)
Experiment (Scale)	**0.5800**	**1.4890**	**3.0690**	**0.0080**
Experiment (Scale-up)	**21.480**	**55.170**	**113.60**	**0.2960**
WAMIT™	**21.140**	**51.700**	**92.450**	**2.3030**
Percentage difference (absolute)	**2%**	**6%**	**19%**	**677%**

on the root mean squared errors (RMS) computations, the values that correspond to the lowest and consistent errors were chosen. As the results, the hydrodynamic damping parameters at velocity 0.55 m/s (for surge), 0.50 m/s (for sway), 0.35 m/s (for heave) and 0.55 rad/s (for yaw) were used.

To obtain the actual results, the following scaling method similar to Table 7 [17, 18] was used to scale up the model. The scaling factor used as shown in (14) was determined heuristically using CFD computations and was independently verified [18]. The scale factors were expressed in matrix form as seen in (14).

$$\left[\begin{array}{ccc|ccc} R^3 & R^3 & R^3 & R^4 & R^4 & R^4 \\ R^3 & R^3 & R^3 & R^4 & R^4 & R^4 \\ R^3 & R^3 & R^3 & R^4 & R^4 & R^4 \\ \hline R^4 & R^4 & R^4 & R^5 & R^5 & R^5 \\ R^4 & R^4 & R^4 & R^5 & R^5 & R^5 \\ R^4 & R^4 & R^4 & R^5 & R^5 & R^5 \end{array}\right] \quad (14)$$

where the dimension of real model to scale model, R is equal to 3.33 for the ROV.

In summary, the measured values of the scale model using the estimated parameters and the theoretical results are tabulated in Table 9. Despite the simple experimental setup, the result obtained is repeatable. Both the theoretical and experimental results indicate that the added mass is smallest in the surge DOF and largest in the heave DOF. This is reasonable given that the vehicle's cross-section area is smallest in the surge than the heave DOF.

However, the percentage difference of the error is quite high for the yaw motion. During the yaw testing, a small change was made to adjust the center of gravity of the scale model when the torsional spring was used. In addition, the scale model was operated on the torsion spring which had some pitching effect. This affects the experimental values for the yaw motion when compared to the WAMIT™ results. However, the simulated responses in the surge, sway and heave motion compare are quite close to the measured responses. Nevertheless, the added mass coefficient in yaw motion can be further improved by enhancing the experimental setup.

V. CONCLUSION

In this paper, the modeling of the hydrodynamic added mass of a complex bluff body like ROV is shown. The added mass coefficients are found to be difficult to obtain since the ROV is nonlinear in dynamics and asymmetry in its design. The computational fluid dynamic software WAMIT™ was used to obtain the added mass coefficients of the ROV model (obtained from MULTISURF™). The free-decaying tests were performed to verify the theoretical results from WAMIT™. The proposed free-decaying test is a viable alternative to estimate pertinent hydrodynamic parameters without extensive and expensive facility and instrumentation before designing the control system. With MATLAB™, the hydrodynamic added mass outputs are displayed. As shown, the experimental results coincide with the simulated results from WAMIT™ with reasonable errors except for the yaw motion. Hence, the proposed systematic method using WAMIT™ is suitable to compute most of the hydrodynamic added mass of a complex-shaped ROV.

For future works, the experimental setup for testing the ROV will be improved. The dynamic thrusters to hull interaction will be included in the study.

REFERENCES

1. Chin, C. and Lau, M., "Modeling and testing of hydrodynamic damping model for a complex-shaped remotely-operated vehicle for control," *Journal of Marine Science and Application*, Vol. 11, No. 2, pp. 150-163 (2012).
2. Chin, C. S., Lau, M. W. S., Low, E., and Seet, G. G. L., "Robust and decoupled cascaded control system of underwater robotic vehicle for stabilization and pipeline tracking," *Proceedings of the Institution of Mechanical Engineers, Part I: Journal of Systems and Control Engineering*, Vol. 222, No. 4, pp. 261-278 (2008).
3. Chin, C. S., Lau, M. W. S., Low, E., and Seet, G. G. L., "A robust controller design method and stability analysis of an underactuated underwater vehicle," *International Journal of Applied Mathematics and Computer Science*, Vol. 16, pp. 345-356 (2006).
4. Eng, Y. H., *Identification of Hydrodynamic Terms for Underwater Robotic Vehicle*, Master of Engineering Dissertation, Robotic Research Center, Mechanical and Aerospace Engineering, NTU (2008).
5. Eng, Y. H., Lau, M. W. S., Low, E., Seet, G. G. L., and Chin, C. S., "Estimation of the hydrodynamic coefficients of an ROV using free decay pendulum motion," *Engineering Letters*, Vol. 16, No. 3, pp. 326-331 (2008).
6. Ferziger, J. H. and Peric, M., *Computational Method for Fluid Dynamics*, Springer, Berlin, pp. 28-50 (2002).
7. Fjellstad, O. E. and Fossen, T. I., "Position and attitude tracking of AUV's: a quaternion feedback approach," *IEEE Journal of Oceanic Engineering*, Vol. 19, No. 4, pp. 512-518 (1994).
8. Fossen, T. I., *Guidance and Control of Ocean Vehicles*, John Wiley & Sons Ltd. (1994).
9. Fossen, T. I., *Marine Control Systems: Guidance, Navigation and Control of Ships, Rigs and Underwater Vehicles*, Marine Cybernetics (2002).
10. Gomes, R. M. F., Sousa, J. B., and Pereira, F. L., "Modelling and control of the IES project ROV," *Proceedings of European Control Conference*,

Cambridge, UK, pp. 1-6 (2003).
11. Goodman, A., "Experimental techniques and methods of analysis used in submerged body research," *Third Symposium on Naval Hydrodynamics*, Scheveningen (1960).
12. Healey, A. J. and Lienard, D., "Multivariable sliding mode control for autonomous diving and steering of unmanned underwater vehicles," *IEEE Journal of Oceanic Engineering*, Vol. 18, No. 3, pp. 327-339 (1993).
13. Jalving, B., "The NDRE-AUV flight controls system," *IEEE Journal of Oceanic Engineering*, Vol. 19, No. 1, pp. 497-501 (1994).
14. Lee, C. H. and Korsmeyer, F. T., *WAMIT User Manual*, Department of Ocean Engineering, MIT (1999).
15. MSS, Marine Systems Simulator, Viewed 26.06.2011, http://www.marinecontrol.org (2010).
16. Ng, E. Y. K. and Tan, C. K., "Viscous flow simulation around a moving projectile and URV," *International Journal of Computer Applications in Technology*, Vol. 11, pp. 350-362 (1998).
17. Prestero, T., *Verification of a Six-Degree of Freedom Simulation Model for the REMUS Autonomous Underwater Vehicle*, Master Thesis, Mechanical and Oceanographic Engineering, Massachusetts Institute of Technology and the Woods Hole Oceanographic Institution (2001).
18. Sarkar, T., Sayer, P. G., and Fraser, S. M., "A study of autonomous underwater vehicle hull forms using computational fluid dynamics," *International Journal for Numerical Methods in Fluids*, Vol. 25, No. 11, pp. 1301-1313 (1997).
19. Tyagi, A. and Sen, D., "Calculation of transverse hydrodynamic coefficients using computational fluid dynamic approach," *Ocean Engineering*, Vol. 33, No. 5, pp. 798-809 (2006).
20. Williams, C. D., Mackay, M., Perron, C., and Muselet, C., "The NRC-IMD marine dynamic test facility: A six-degree-of-freedom forced-motion test apparatus for underwater vehicle testing," *International UUV Symposium*, Newport RI, IR-1999-28 (2000).
21. Wilson, R., Paterson, E., and Stern, F., "Unsteady RANS CFD method for naval combatant in waves," *Proceedings of the 22nd ONR Symposium on Naval Hydrodynamics*, Washington DC, National Academy Press, pp. 532-549 (2006).
22. WS Atkins *Consultants, Best Practices Guidelines for Marine Applications of CFD*, MARNET-CFD Report (2002).